

On the extremal spectral properties of random graphs

C. T. Martínez-Martínez^{1,2} and J. A. Méndez-Bermúdez³

¹*Universidad Autónoma de Guerrero, Centro Acapulco CP 39610, Acapulco de Juárez, Guerrero, Mexico*

²*Facultad de ciencias. Universidad Autónoma Benito Juárez de Oaxaca, Oaxaca de Juárez CP 68120, Oaxaca, Mexico*

³*Instituto de Física, Benemérita Universidad Autónoma de Puebla, Puebla 72570, Mexico*

(Dated: June 17, 2025)

In this work, we study some statistical properties of the extreme eigenstates of the randomly-weighted adjacency matrices of random graphs. We focus on two random graph models: Erdős-Rényi (ER) graphs and random geometric graphs (RGs). Indeed, the adjacency matrices of both graph models are diluted versions of the Gaussian Orthogonal Ensemble (GOE) of random matrix theory (RMT), such that a transition from the Poisson Ensemble (PE) and the GOE is observed by increasing the graph average degree $\langle k \rangle$. First, we write down expressions for the spectral density in terms of $\langle k \rangle$ for the regimes below and above the percolation threshold. Then, we show that the distributions of both, the largest λ_1 and second-largest λ_2 eigenvalues approach the Tracy-Widom distribution of type 1 for $\langle k \rangle \gg 1$, while $\langle \lambda_1 \rangle = \sqrt{2\langle k \rangle}$. Additionally, we demonstrate that the distributions of the normalized distance between λ_1 and λ_2 , the distribution of the ratio between higher consecutive eigenvalues spacings, as well as the distributions of the inverse participation ratios of the extreme eigenstates display a clear PE-to-GOE transition as a function of $\langle k \rangle$, so any of these distributions can be effectively used to probe the delocalization transition of the graph models without the need of the full spectrum.

PACS numbers:

I. INTRODUCTION

The spectrum of a graph is the set of eigenvalues of the corresponding adjacency matrix. Within the study of spectral properties of graphs, a relevant direction is the analysis of extremal spectral quantities, such as the principal eigenvalue or largest eigenvalue λ_1 [1–5]. The largest eigenvalue is a relevant quantity in various contexts, not only for graphs and networks, as it is associated with important properties such as stability, dynamic response, and certain structural characteristics of the corresponding system. In mechanical and structural engineering, for example, knowing the largest eigenvalue of the stiffness or mass matrix (which is related to the highest natural frequency of the system) is important to avoid destructive resonances [6–9]. In finance, the largest eigenvalue of the asset return covariance matrix informs about risk concentration and helps construct optimal portfolios [10–12]. In physics, particularly in the study of disordered systems and quantum chaos, the behavior of the largest eigenvalue of a Hamiltonian is key to understanding phenomena such as Anderson localization and the distribution of energy levels in complex quantum systems [13–16]. In graphs and networks, the largest eigenvalue of the corresponding adjacency matrix provides a measure of the connectivity of the system. It can indicate structural characteristics such as hubs, communities, or the presence of dominant nodes [17, 18]. It also influences the determination of dynamic properties, such as the threshold for epidemic propagation or synchronization [19–21]. As for the Laplacian matrix, its largest eigenvalue carries complementary information. While the smallest non-zero Laplacian eigenvalue is commonly studied due to its connection to network robustness and communication efficiency, the largest Laplacian

eigenvalue is also significant. It governs the upper bound of the spectrum and is linked to the network's ability to synchronize in dynamical processes. In particular, the ratio between the largest and the second-smallest Laplacian eigenvalues (the spectral gap) is a key factor in assessing synchronizability in systems of coupled oscillators [19]. Moreover, the largest Laplacian eigenvalue can reflect structural heterogeneity and can be used to bound quantities like the chromatic number or the isoperimetric number of the graph [18]. Thus, the spectrum of the adjacency matrix and the Laplacian provides relevant information about the structure and dynamics of complex networks, and the extreme eigenvalues are important in characterizing these properties.

The spectrum of the binary adjacency matrix of Erdős-Rényi graphs has been widely studied, see for example [1, 22]. In the binary case, there is a significant difference between the statistical properties of the spectrum's bulk and the spectrum's edges. It is known that the expected value of the largest eigenvalue λ_1 scales as Np when $Np \gg \log(N)$, where N is the number of nodes and p the connection probability. This arises because the standard binary adjacency matrix of the Erdős-Rényi model resembles a random matrix whose average degree $\langle k \rangle = Np$ governs its spectral properties [3].

However, in this work, we consider randomly-weighted adjacency matrices, which makes previous results not directly applicable. The random weights we incorporate into the graph's adjacency matrices follow a Gaussian distribution with mean zero and unit variance. Thus, these adjacency matrices can be interpreted as diluted versions of matrices from the Gaussian Orthogonal Ensemble (GOE) of random matrix theory (RMT) [16]. For the GOE, as $N \rightarrow \infty$, the largest eigenvalue λ_1 follows the Tracy-Widom distribution of type 1, which is known

to characterize the fluctuations of extremal eigenvalues of large random matrices [23].

Thus, in this work, we focus on the study of spectral properties of graphs using tools from RMT, with particular emphasis on extremal spectral characteristics. Specifically, we explore some statistical properties of the largest eigenvalue λ_1 . For this purpose, we consider two models of random graphs: The Erdős-Rényi random graph model and the random geometric graph model.

This paper is organized as follows. In Section II, we analyze the spectral properties of the Erdős-Rényi model, beginning with a brief description of the model, followed by a study of its spectral density, the behavior of the largest eigenvalue, and the characteristics of the corresponding eigenvectors. In Appendix A, we extend the analysis to the random geometric graph model, presenting analogous results. Finally, in Section III, we summarize and discuss the main findings for both models.

II. ERDŐS-RÉNYI MODEL

A. Model

An Erdős-Rényi (ER) graph, denoted by $G(N, p)$, is an undirected random graph with N independent vertices connected with probability p . Given two vertices u and v , p is the probability of an edge from vertex u to vertex v , so $p \in [0, 1]$. When $p = 0$, the graph consists of N isolated vertices; when $p = 1$, it becomes a complete graph. We can generate graphs between these two extremes by varying the value of p between 0 and 1. It is important to note that a given pair of parameters (N, p) represents an infinite set of random graphs. Therefore, calculating a given property for a single graph may not be representative of the entire model. Instead, we can obtain more relevant information by calculating the average of that property over an ensemble of random graphs characterized by the same pair of parameters (N, p) . Although this statistical approach is a common practice in RMT, it is not as common in graph theory; however, it has been recently applied to several random graph models [24–30].

As already said above, in this work we study spectral properties of ER graphs. Moreover, to enable the comparison with standard results from RMT, we assign Gaussian random weights to the entries of the adjacency matrix \mathbf{A} of $G(N, p)$ as

$$A_{ij} = \begin{cases} \sqrt{2}\epsilon_{ii} & \text{for } i = j, \\ \epsilon_{ij} & \text{if there is an edge between vertices } i \text{ and } j, \\ 0 & \text{otherwise.} \end{cases} \quad (1)$$

Here, we choose ϵ_{ij} as statistically independent random variables drawn from a normal distribution with zero mean and variance one. Also, $\epsilon_{ij} = \epsilon_{ji}$, since G is undirected. According to this definition, diagonal random matrices are obtained for $p = 0$ (Poisson ensemble (PE) in RMT terms), whereas the GOE (i.e. full real and sym-

metric random matrices) is recovered when $p = 1$ [16]. Therefore, a transition from the PE to the GOE can be observed by increasing p from zero to one for any given graph size N . Indeed, to characterize this PE-to-GOE transition, several RMT measures based on the eigenvalues and eigenvectors of the adjacency matrix of Eq. (1) have already been used; see e.g. Refs. [32–35].

In what follows, we call the ER random graphs represented by the randomly-weighted adjacency matrix of Eq. (1) as *randomly-weighted ER graphs*.

B. Spectral Density

We first examine the spectrum of randomly-weighted ER graphs by calculating the spectral density, which is the distribution of eigenvalues of the adjacency matrix. Indeed, for a finite graph, the spectral density can be expressed as a sum of Dirac delta functions:

$$\rho(\lambda) := \frac{1}{N} \sum_{j=1}^N \delta(\lambda - \lambda_j), \quad (2)$$

where λ_j is the j -th eigenvalue of the graph's adjacency matrix.

A well-known result in RMT is Wigner's semicircle law [36]. This law states that for a real, symmetric, $N \times N$ random matrix A with uncorrelated elements, where $\langle A_{ij} \rangle = 0$ and $\langle A_{ij}^2 \rangle = \sigma^2$ for $i \neq j$, and where each moment of $|A_{ij}|$ remains finite as N increases, the spectral density of A/\sqrt{N} converges to the semicircular distribution

$$\rho(\lambda) = \begin{cases} (2\pi\sigma^2)^{-1} \sqrt{4\sigma^2 - \lambda^2} & \text{if } |\lambda| < 2\sigma, \\ 0 & \text{otherwise,} \end{cases} \quad (3)$$

in the limit $N \rightarrow \infty$.

Therefore, we expect the spectrum of randomly-weighted ER graphs to approach Wigner's semicircle law when $p \rightarrow 1$. In contrast, notice that when $p \rightarrow 0$, the adjacency matrices are diagonal with random entries drawn from a Gaussian distribution, resulting in a spectral density following that Gaussian distribution. Thus, in the transition from isolated to complete graphs, we expect to observe the transition from a Gaussian spectral density to the Wigner's semicircle law. For intermediate values of p , the average variance of the elements of the adjacency matrix is strongly affected by the number of elements equal to zero, which is closely related to the average degree of the graph.

The degree of a node is the number of edges connected to it. According to several studies, see e.g. [24–30, 32], the average degree is a quantity that characterizes several spectral and topological properties of graphs and networks. In the case of ER-type graphs, the average degree is given by

$$\langle k \rangle = (N - 1)p. \quad (4)$$

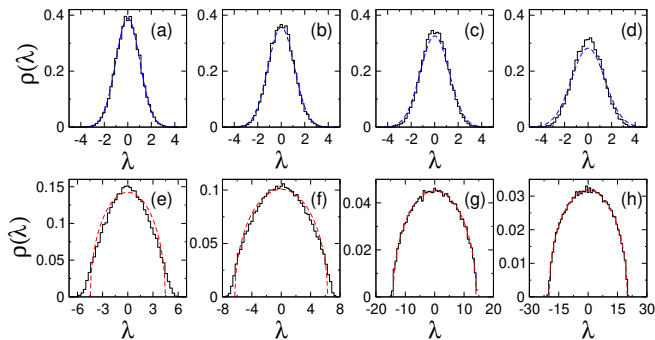


FIG. ERGs1: Spectral density of randomly-weighted Erdős-Rényi graphs of size $N = 200$ and (a) $\langle k \rangle = 1.05$, (b) $\langle k \rangle = 1.25$, (c) $\langle k \rangle = 1.5$, (d) $\langle k \rangle = 2$, (e) $\langle k \rangle = 10$, (f) $\langle k \rangle = 20$, (g) $\langle k \rangle = 100$, and (h) $\langle k \rangle = 200$. Blue and red dashed lines correspond to Eqs. (6) and (7), respectively. The eigenvalues of 100 adjacency matrices were used to construct each histogram.

However, in our specific case, the graphs include self-loops, which means that even when the connection probability p is zero, each node is still connected to itself. This results in a modified expression for the average degree:

$$\langle k \rangle = 1 + (N - 1)p. \quad (5)$$

The random weights of the adjacency matrix \mathbf{A} have unit variance. However, for decreasing connection probability, the number of zero entries in the adjacency matrix increases, effectively reducing the overall variance of the matrix. This variance reduction can be directly connected to the average degree $\langle k \rangle$. In particular, since the model includes self-connections, the percolation threshold is reached at $\langle k \rangle = 2$; at this point, connected components emerge more frequently. Specifically, we find that $\sigma = \langle k \rangle$ for $\langle k \rangle < 2$, while $\sigma = \langle k \rangle / 2$ for $\langle k \rangle > 2$.

So, following Wigner's law and considering the relationship between variance and average degree, we propose the following expression for the spectral density of randomly-weighted ER graphs:

$$\rho(\lambda) = \frac{1}{\sqrt{2\pi\langle k \rangle}} \exp\left(-\frac{\lambda^2}{2\langle k \rangle}\right), \quad (6)$$

if $\langle k \rangle < 2$, while

$$\rho(\lambda) = \begin{cases} (\pi\langle k \rangle)^{-1} \sqrt{2\langle k \rangle - \lambda^2} & \text{if } |\lambda| < \sqrt{2\langle k \rangle}, \\ 0 & \text{otherwise,} \end{cases} \quad (7)$$

if $\langle k \rangle > 2$. In Fig. ERGs1, we present the spectral density of randomly-weighted ER graphs for several values of $\langle k \rangle$, as specified in the caption. Indeed, Eqs. (6) (blue lines) and (7) (red lines) fit the distributions well for small and large values of $\langle k \rangle$, respectively.

From Fig. ERGs1 we observe that, unlike the binary case, for randomly-weighted ER graphs there is no clear separation between the largest and second-largest eigenvalues. Furthermore, for large values of $\langle k \rangle$, the largest

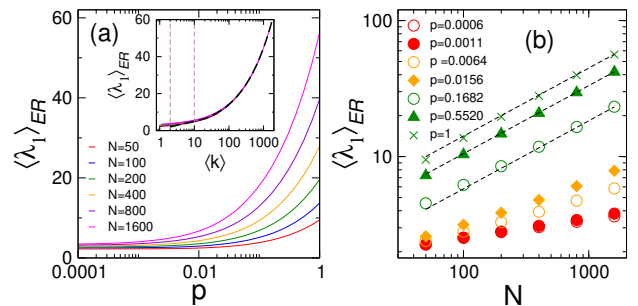


FIG. ERGs2: (a) The average largest eigenvalue $\langle \lambda_1 \rangle$, of randomly-weighted Erdős-Rényi graphs, as a function of the connection probability p . Inset: $\langle \lambda_1 \rangle$ as a function of the average degree $\langle k \rangle$. (b) $\langle \lambda_1 \rangle$ as a function of the graph size N for different values of p , as indicated in the panel. Dashed lines in the inset of panel (a) and in panel (b) correspond to Eq. (8). Each symbol was calculated by averaging over $10^6/N$ random graphs.

eigenvalue appears to be directly related to the radius of the spectral density. Next, we analyze the behavior of the largest eigenvalue as a function of the model parameters.

C. Largest eigenvalue

In Figs. ERGs2(a) and ERGs2(b) we plot the average largest eigenvalue $\langle \lambda_1 \rangle$ of randomly-weighted ER graphs as a function of p and N , respectively. In the inset of Fig. ERGs2(a), we present $\langle \lambda_1 \rangle$ as a function of the average degree and observe that it depends solely on it. Moreover, according to Eq. (7), the largest eigenvalue can be expressed as

$$\lambda_1 = \sqrt{2\langle k \rangle}. \quad (8)$$

The inset of Fig. ERGs2(a) shows that Eq. (8) (dashed black line) provides a good description of the numerical data for $k > 2$, which works even better for $k > 10$ (brown dashed line). Fig. ERGs2(b) shows the average largest eigenvalue $\langle \lambda_1 \rangle$ as a function of the network size N for different values of the connection probability p , as indicated in the legend. Green symbols correspond to higher values of p , while red symbols indicate lower values. We can see that $\langle \lambda_1 \rangle$ follows a power-law dependence on N . Based on Eq. (8), by substituting the expression for the average degree, we obtain the approximation $\lambda_1 \approx \sqrt{2Np}$. This approximation is indicated by dashed lines in the figure, particularly for higher values of p . We observe that this approximation agrees better with the numerical results when p is bigger.

Moreover, we also explore the distribution of λ_1 for different parameter combinations. To ease the comparison of results, we normalize the largest eigenvalue as:

$$\tilde{\lambda}_1 = \frac{\lambda_1 - \langle \lambda_1 \rangle}{\sigma_{\lambda_1}} \quad (9)$$

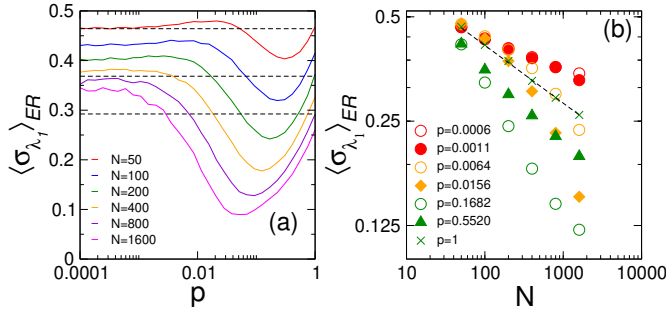


FIG. ERGs3: (a) The average variance of the largest eigenvalue $\langle \sigma_{\lambda_1} \rangle$, of randomly-weighted Erdős-Rényi graphs, as a function of the connection probability p . (b) $\langle \sigma_{\lambda_1} \rangle$ as a function of the graph size N for different values of p , as indicated in the panel. Dashed lines in (a) correspond to $N^{-1/6}$ for $N = 100, 400$ and 1600 . Dashed line in (b) is $N^{-1/6}$. Each symbol was calculated by averaging over $10^6/n$ random graphs.

where $\langle \lambda_1 \rangle$ is the mean value of the largest eigenvalue and σ_{λ_1} its standard deviation.

Figure ERGs3 shows the average variance of the largest eigenvalue $\langle \sigma_{\lambda_1} \rangle$ of randomly-weighted ER graphs as a function of (a) p and (b) N . From Fig. ERGs3(a) we can see that $\langle \sigma_{\lambda_1} \rangle$ is not a simple function of p : For small p it remains almost constant, then decreases as p grows, reaching a minimum, and finally increases with p . As a function of the graph size N , see Fig. ERGs3(b)), $\langle \sigma_{\lambda_1} \rangle$ follows a decreasing power law, where the power law depends on the value of p .

For the GOE, when $N \rightarrow \infty$, the largest normalized eigenvalue $\tilde{\lambda}_1$ follows a distribution that converges to the Tracy-Widom distribution of type 1 [23]. In fact, for the GOE, the asymptotic expected value of the largest eigenvalue is given by $\langle \lambda_1 \rangle = \sqrt{2N}$ and the scale of fluctuations around this expected value is given by $\sigma_{\lambda_1} = N^{-1/6}$ for large matrices; this value has been plotted in dotted lines in Fig. ERGs3(a) for $n = 100, 400$ and 1600 . More specifically, if λ_1 is the largest eigenvalue of a GOE $N \times N$ matrix, then the distribution of

$$\tilde{\lambda}_1 = \frac{\lambda_1 - \sqrt{2N}}{N^{-1/6}} \quad (10)$$

converges to the Tracy-Widom distribution of type 1.

Then, in Fig. ERGs4 (top panels), we present distributions of the largest eigenvalue $P(\tilde{\lambda}_1)$ of randomly-weighted ER graphs. λ_1 is normalized according with Eq. (9). Given that the average degree serves as a scaling parameter of several structural and spectral properties of graphs [26, 30–32], we decided to examine $P(\tilde{\lambda}_1)$ for fixed values of $\langle k \rangle$. To this end, we choose values of $\langle k \rangle$ from weakly to highly connected graphs: $\langle k \rangle = 1.25, 5, 50$, and 100 ; as indicated on top of the panels. In addition, in Fig. ERGs4 (lower panels), we present distributions of the second-largest eigenvalue. We note that the distributions of both (normalized) eigenvalues tend to the

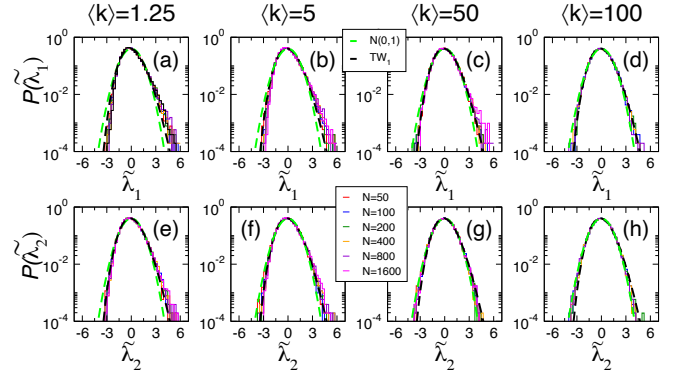


FIG. ERGs4: Top panels: Distributions of the largest eigenvalue $P(\tilde{\lambda}_1)$ of randomly-weighted Erdős-Rényi graphs for different values of $\langle k \rangle$, as indicated at the top of the panels. Bottom panels: Distributions of the second largest eigenvalue $P(\tilde{\lambda}_2)$. Each panel includes histograms for several graph sizes $n \in [50, 400]$. Black and green dashed lines correspond to the Tracy-Widom distribution of type 1 and normal distributions, respectively. Each histogram was constructed from $10^6/n$ random graphs.

Tracy-Widom distribution of type 1 for increasing $\langle k \rangle$, see the green dashed lines in Fig. ERGs4(d,h).

To better characterize the overall behavior of the eigenvalue distributions of Fig. ERGs4, we compute their excess kurtosis and skewness. Then, in Figs. ERGs5(a) and ERGs5(b), respectively, we plot the excess kurtosis and the skewness of the distribution of the largest eigenvalue λ_1 as a function of the connection probability p of randomly-weighted ER graphs. Both quantities are normalized to the corresponding values of the Tracy-Widom distribution of type 1, which is approached when $p \rightarrow 1$; see Fig. ERGs4. In Figs. ERGs5(c) and ERGs5(d) we also plot the excess kurtosis and the skewness of $P(\lambda_2)$, respectively.

From Figs. ERGs5(a) and ERGs5(b), when p is small, we observe that the excess kurtosis and skewness of $P(\lambda_1)$ deviate considerably from the Tracy-Widom value. However, as p increases, as expected, both quantities progressively approach the reference Tracy-Widom values; although fluctuations persist at large values of p . In the case of $P(\lambda_2)$, the situation is different: While both the excess kurtosis and the skewness decrease with p , they do not approach the reference Tracy-Widom values; see Figs. ERGs5(c) and ERGs5(d). This may be expected, even with the apparent good correspondence between $P(\lambda_2)$ and the Tracy-Widom distribution shown in Fig. ERGs4(h), since Tracy-Widom-type statistics is expected for λ_1 only.

Now, we also compute the correlation coefficient between the first and second eigenvalues, c_{λ_1, λ_2} , defined by

$$c_{\lambda_1, \lambda_2} = \langle \tilde{\lambda}_1 \tilde{\lambda}_2 \rangle - \langle \tilde{\lambda}_1 \rangle \langle \tilde{\lambda}_2 \rangle. \quad (11)$$

c_{λ_1, λ_2} as a function of p of randomly-weighted ER graphs is shown in Fig. ERGs6. From this figure, we observe

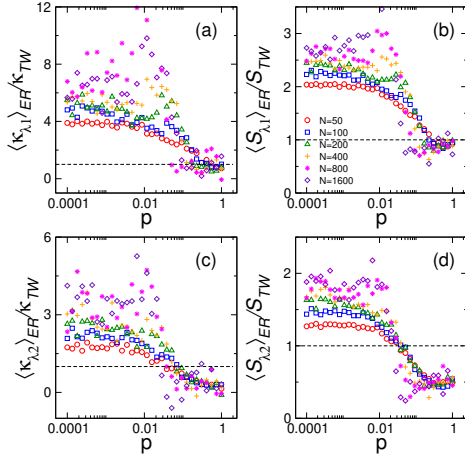


FIG. ERGs5: (a) [(c)] Excess kurtosis and (b) [(d)] skewness, normalized to the corresponding values of the Tracy-Widom distribution of type 1, of the distribution of the largest eigenvalue λ_1 [of the distribution of the second largest eigenvalue λ_2] as a function of the connection probability p of randomly-weighted Erdős-Rényi graphs of sizes $n \in [50, 400]$. Each symbol was computed by averaging over $10^6/n$ random graphs.

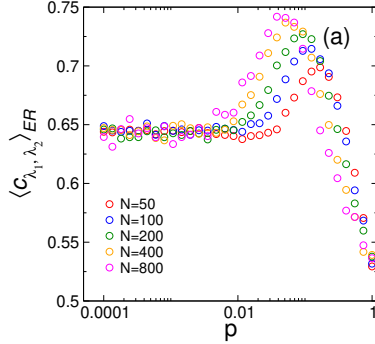


FIG. ERGs6: Correlation coefficient between the largest and the second largest eigenvalues as a function of the connection probability p of randomly-weighted Erdős-Rényi graphs of sizes $n \in [50, 400]$. Each symbol was computed by averaging over $10^6/n$ random graphs.

that, for small p , the correlation coefficient remains approximately constant and close to $c_{\lambda_1, \lambda_2} = 0.65$. This may be regarded as the PE value. Then, for further increasing p , c_{λ_1, λ_2} grows, reaches a maximum, and finally decreases until reaching the predicted value for the GOE, $c_{\lambda_1, \lambda_2} \approx 0.53$ [5].

From the results presented so far, we have observed that the statistical properties of the largest eigenvalue (and also of the second largest eigenvalue) of the model of randomly-weighted ER graphs shows a clear PE-to-GOE transition as a function of the graph connectivity, or more precisely, as a function of the average degree. Although the PE-to-GOE transition as a function of $\langle k \rangle$ has been reported previously by the use of the full spectrum, see e.g. [24], it is important to highlight that our results demonstrate that the PE-to-GOE transition could

also be probed by the use of the extreme eigenvalues only. To further verify this statement, we now compute the distribution of the normalized distance between the largest and second-largest eigenvalues, defined as

$$s = \frac{\lambda_1 - \lambda_2}{\langle \lambda_1 - \lambda_2 \rangle}, \quad (12)$$

and the distribution of the ratio between higher consecutive eigenvalues spacings

$$r = \frac{\min(\lambda_1 - \lambda_2, \lambda_2 - \lambda_3)}{\max(\lambda_1 - \lambda_2, \lambda_2 - \lambda_3)}. \quad (13)$$

In Fig. ERGs7 we present $P(s)$ (top panels) and $P(r)$ (bottom panels) of randomly-weighted ER graphs for different values of $\langle k \rangle$, as indicated at the top of the panels. Note that we are using the same values of $\langle k \rangle$ reported in Fig. ERGs4. In Fig. ERGs7 we are also including the RMT predictions of both $P(s)$ and $P(r)$ for the PE and the GOE, which are given by

$$P_{\text{PE}}(s) = \exp(-s), \quad (14)$$

$$P_{\text{PE}}(r) = \frac{2}{(1+r)^2}, \quad (15)$$

$$P_{\text{GOE}}(s) = \frac{\pi}{2} s \exp\left(-\frac{\pi}{4} s^2\right), \quad (16)$$

and

$$P_{\text{GOE}}(r) = \frac{27}{4} \frac{(r+r^2)}{(1+r+r^2)^{5/2}}. \quad (17)$$

However, it is important to stress that Eqs. (14-17) are expected to work at the bulk of the spectrum. Then, from Fig. ERGs7 we observe that: (i) for fixed $\langle k \rangle$ the shape of both $P(s)$ and $P(r)$ remains invariant, i.e. they do not depend on the graph size; except for intermediate values of $\langle k \rangle$, see Figs. ERGs7(b,f); (ii) for small [large] values of $\langle k \rangle$, the shapes of $P(s)$ and $P(r)$ are well described by $P_{\text{PE}}(s)$ and $P_{\text{PE}}(r)$ [$P_{\text{GOE}}(s)$ and $P_{\text{GOE}}(r)$], respectively; (iii) both $P(s)$ and $P(r)$ can be used to probe the PE-to-GOE transition.

D. Eigenvector properties

To further explore the properties of the edge of the spectrum, here we compute the inverse participation ratio (IPR) of the eigenvectors corresponding to the extreme eigenvalues. Given the normalized eigenvectors Ψ^i , its IPR is defined as

$$\text{IPR}_i = \left[\sum_{m=1}^N |\Psi_m^i|^4 \right]^{-1}. \quad (18)$$

In fact, we compute distributions of IPRs of eigenvectors of randomly-weighted ER graphs, as shown in

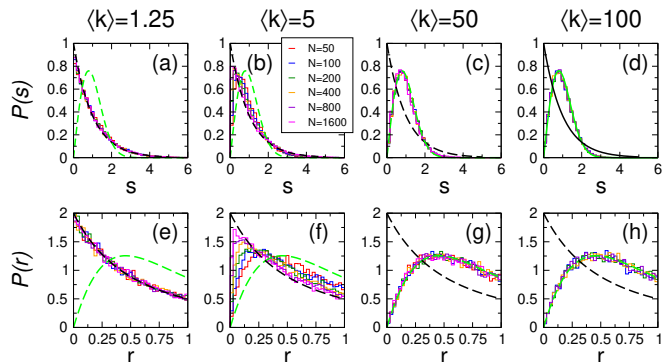


FIG. ERGs7: Top panels: Distribution of the normalized distance between the largest and second-largest eigenvalues $P(s)$ of randomly-weighted Erdős-Rényi graphs for different values of $\langle k \rangle$, as indicated at the top of each panel. Bottom panels: Distribution of the ratio between higher consecutive eigenvalues spacings $P(r)$. Each panel displays histograms for different graph sizes, $n \in [50, 400]$. In the top panels, black and green dashed lines correspond to Eqs. (14) and (16), respectively. In the bottom panels, black and green dashed lines correspond to Eqs. (15) and (17), respectively. Each histograms was constructed from $10^6/n$ random graphs.

Fig. ERGs8. Notice that each column in Fig. ERGs8 corresponds to a fixed value of $\langle k \rangle$; we used the same values of $\langle k \rangle$ reported in Figs. ERGs4 and ERGs7. Specifically, in Fig. ERGs8 we show the distributions of the IPRs of the eigenvectors corresponding to the largest eigenvalue, see panels (a-d), and to the second largest eigenvalue, see panels (e-h). Moreover, for comparison purposes, we also show $P(\text{IPR})$ of the eigenvectors corresponding to the central eigenvalue, see panels (i-l), the smallest eigenvalue, see panels (m-p), and the average IPR over the full spectrum, see panels (q-t).

From Fig. ERGs8 we observe that all IPR distributions display a clear delocalization transition as the average degree of the graph increases. For small values of $\langle k \rangle$, see the left panels corresponding to $\langle k \rangle = 5$, the IPR distributions show a pronounced peak at $\text{IPR} = 3$, a signature of strongly localization and a characteristic of the PE. For large values of $\langle k \rangle$, see the right panels corresponding to $\langle k \rangle = 100$, the IPR distributions follow a Gaussian-like bell shape centered at $\text{IPR} \propto N$, indicating delocalization which is the main characteristic of the GOE. For intermediate values of $\langle k \rangle$, we observe a transition between the PE and the GOE regimes. The eigenvectors corresponding to the extreme eigenvalues (largest, second largest, and smallest) exhibit similar localization characteristics. This, in contrast with the eigenvector corresponding to the central eigenvalue $\lambda_{N/2}$, which also displays the delocalization transition but in a different manner. The distributions of the average IPR, shown in panels (q-t), included for comparison purposes, clearly show that, on average, the localization properties of the bulk eigenvalues dominate.

We recall then that the localization properties of the

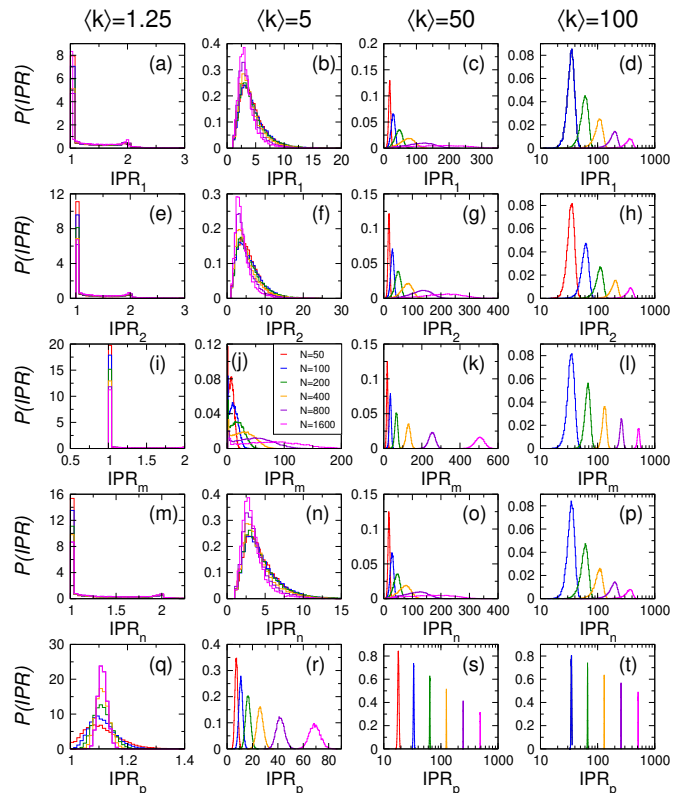


FIG. ERGs8: Distributions of inverse participation ratios $P(\text{IPR})$ of eigenstates of randomly-weighted Erdős-Rényi graphs of sizes $N \in [50, 800]$. Each column corresponds to a fixed value of $\langle k \rangle$. Rows are $P(\text{IPR})$ of eigenstates corresponding to: (a-d) the largest eigenvalue, (e-h) the second largest eigenvalue, (i-l) the central eigenvalue ($m = N/2$), (m-p) the smallest eigenvalue, and (q-t) the average IPR over the full spectrum.

eigenvectors are not uniform across the spectrum. In general, the eigenvectors at the center of the spectrum are more delocalized than those at the edges. Also, extreme states tend to be more closely aligned with the topological structure of the graph than those at the spectrum center, see e.g. [1]. Indeed, the spectral heterogeneity is key to understanding dynamical processes in graphs, such as diffusion, synchronization, or stability, where different modes can have differentiated contributions depending on their degree of localization; see e.g. [19, 20].

III. CONCLUSIONS AND DISCUSSION

In this paper, we have studied some statistical properties of the extreme eigenstates of randomly-weighted adjacency matrices \mathbf{A} corresponding to two random graph models: Erdős-Rényi (ER) graphs and random geometric graphs (RGGs). Since we added self-connections to the graph's nodes, see Eq. (1), the adjacency matrices of both graph models are diluted versions of the Gaussian Orthogonal Ensemble (GOE) of random matrix theory

(RMT), such that a transition from the Poisson Ensemble (PE) and the GOE is observed by increasing the graph average degree $\langle k \rangle$. We note that, to avoid saturation of the main text, the results for randomly-weighted RGGs are reported in the Appendix.

First, we wrote down expressions for the spectral density in terms of $\langle k \rangle$ for the regimes below and above the percolation threshold; see Eqs. (6) and (7), respectively, and Figs. ERGs1 and RGGs1. Then, we showed that the average value of the largest eigenvalue $\langle \lambda_1 \rangle$ depends on $\langle k \rangle$ only and it is well described by Eq. (8); see the insets in Figs. ERGs2(a) and RGGs2(a). Moreover, we verified that both distributions, $P(\lambda_1)$ and $P(\lambda_2)$ (the distribution of the second-largest eigenvalue), approach the Tracy-Widom distribution of type 1 for $\langle k \rangle \gg 1$; see Figs. ERGs4 and RGGs4.

We also demonstrated that the distributions of the normalized distance between λ_1 and λ_2 , $P(s)$, the distribution of the ratio between higher consecutive eigenvalues spacings, $P(r)$, as well as the distributions of the inverse participation ratios of the extreme eigenstates display a clear PE-to-GOE transition as a function of $\langle k \rangle$, so any of these distributions can be effectively used to probe the delocalization transition of the graph models without the need of the full spectrum. Moreover, for small [large] values of $\langle k \rangle$, the shapes of $P(s)$ and $P(r)$ are well described by the RMT predictions $P_{\text{PE}}(s)$ and $P_{\text{PE}}(r)$ [$P_{\text{GOE}}(s)$ and $P_{\text{GOE}}(r)$], respectively; see Figs. ERGs7 and RGGs7.

These findings demonstrate the relevance of extreme spectral statistics as indicators of transitions in complex networks. In particular, they suggest that important information about the connectivity regime and overall system behavior can be obtained from just a few spectral observables. This is particularly beneficial in problems where accessing the full spectrum is computationally expensive. Future research could explore whether these indicators remain effective in characterizing other types of networks with more specific structures, as well as their relevance to real-world networks and dynamics, such as diffusion, synchronization, or signal propagation.

Appendix A: Random geometric graphs

In this Appendix, we report the statistical properties of the extreme states of the randomly-weighted adjacency matrices of random geometric graphs (RGGs).

The model of RGGs is defined as follows: N nodes are distributed uniformly over a square with unit side. Then, if the distance between two nodes is less than a connection radius r , an edge is set between them. When $r = 0$ the graph is completely disconnected, while if $r = \sqrt{2}$ the graph is complete. This model is then defined by the parameters N , the total number of nodes or size of the graph, and r , the connection radius.

For RGGs, the expression for average degree is more complex than that for ER graphs. For RGGs, without

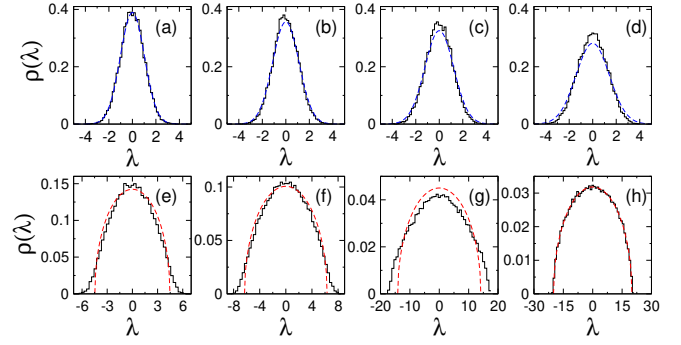


FIG. RGGs1: Spectral density of randomly-weighted random geometric graphs of size $N = 200$ and (a) $\langle k \rangle = 1.05$, (b) $\langle k \rangle = 1.25$, (c) $\langle k \rangle = 1.5$, (d) $\langle k \rangle = 2$, (e) $\langle k \rangle = 10$, (f) $\langle k \rangle = 20$, (g) $\langle k \rangle = 100$, and (h) $\langle k \rangle = 200$. Blue and red dashed lines correspond to Eqs. (6) and (7), respectively. The eigenvalues of 100 adjacency matrices were used to construct each histogram.

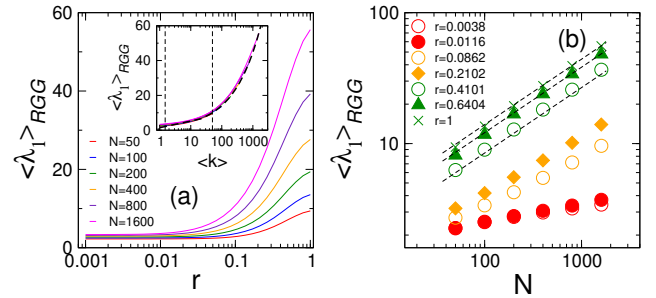


FIG. RGGs2: (a) The average largest eigenvalue $\langle \lambda_1 \rangle$, of randomly-weighted random geometric graphs, as a function of the connection radius r . Inset: $\langle \lambda_1 \rangle$ as a function of the average degree $\langle k \rangle$. (b) $\langle \lambda_1 \rangle$ as a function of the graph size N for different values of r , as indicated in the panel. Dashed lines in the inset of panel (a) and in panel (b) correspond to Eq. (8). Each symbol was calculated by averaging over $10^6/N$ random graphs.

self-connections, the average degree is given by [37]:

$$\langle k \rangle = (N - 1)F(r), \quad (\text{A1})$$

where

$$F(r) = \begin{cases} \pi r^2 - \frac{4}{3}r^3 + \frac{1}{2}r^4 & \text{for } 0 < r \leq 1, \\ \frac{1}{3} - \frac{1}{2}r^4 + \left(\frac{8}{3}r^2 + \frac{4}{3}\right)\sqrt{r^2 - 1} - 2r^2 \left(\arccos\left(\frac{1}{r}\right) - \arcsin\left(\frac{1}{r}\right) + 1\right) & \text{for } r > 1. \end{cases} \quad (\text{A2})$$

We use the same approach as for the randomly-weighted ER graphs; that is, we add self-connections to the nodes and random weights to the corresponding adjacency matrix. Under these conditions, the average degree is written as

$$\langle k \rangle = 1 + (N - 1)F(r). \quad (\text{A3})$$

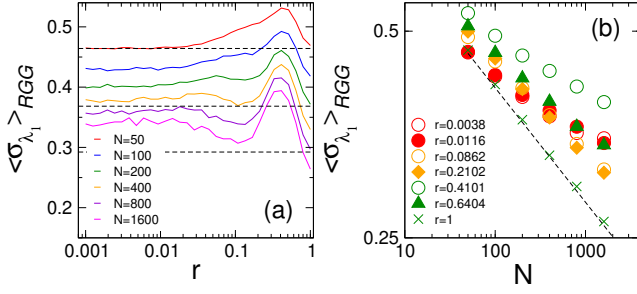


FIG. RGGs3: (a) The average variance of the largest eigenvalue $\langle \sigma_1 \rangle$, of randomly-weighted random geometric graphs, as a function of the connection radius r . (b) $\langle \sigma_1 \rangle$ as a function of the graph size N for different values of r , as indicated in the panel. Dashed lines in (a) correspond to $N^{-1/6}$ for $N = 100, 400$ and 1600 . Dashed line in (b) is $N^{-1/6}$. Each symbol was calculated by averaging over $10^6/n$ random graphs.

1. Results

Our results for randomly-weighted RGGs are presented in Figs. RGGs1–RGGs8. Note that Figs. RGGs1–RGGs8 for randomly-weighted RGGs are equivalent to Figs. ERGs1–ERGs8 for randomly-weighted ER graphs, respectively. Indeed, from Figs. RGGs1–RGGs8 we draw similar conclusions as those already discussed in the main text for randomly-weighted ER graphs:

- (i) The spectral density of randomly-weighted RGGs has a Gaussian shape for $\langle k \rangle < 2$ and a semicircular shape for $\langle k \rangle > 2$ as given by Eqs. (6) and (7), respectively; see Fig. RGGs1. However, significant deviations are observed for given values of $\langle k \rangle$; see e.g. Fig. RGGs1(g), which may need further exploration.
- (ii) The average largest eigenvalue $\langle \lambda_1 \rangle$ of randomly-weighted RGGs depends on the average degree as given by Eq. (8); see the inset of Fig. RGGs2(a) and Fig. RGGs2(b).
- (iii) The average variance of the largest eigenvalue exhibits a power-law dependence on network size; see Fig. RGGs3 (b), with an exponent that varies with the connection radius. This variation becomes particularly noticeable for $r > 0.1$ as reflected in the bell-shaped behavior shown in Fig. RGGs3 (a).
- (iv) The distributions of the largest eigenvalue $P(\lambda_1)$ and of the second largest eigenvalue $P(\lambda_2)$ of randomly-weighted RGGs approach a Tracy-Widom distribution of type 1 for $r \rightarrow \sqrt{2}$ (or $\langle k \rangle \gg 1$); see Figs. RGGs4 and RGGs5.
- (vi) The correlation coefficient between the largest and the second largest eigenvalues of randomly-weighted RGGs displays the PE-to-GOE transition as a function of r . That is, $c_{\lambda_1, \lambda_2} \approx 0.65$

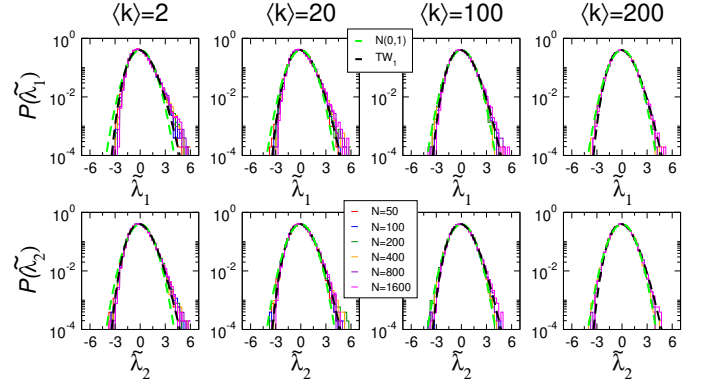


FIG. RGGs4: Top panels: Distributions of the largest eigenvalue $P(\lambda_1)$ of randomly-weighted random geometric graphs for different values of $\langle k \rangle$, as indicated at the top of the panels. Bottom panels: Distributions of the second largest eigenvalue $P(\lambda_2)$. Each panel includes histograms for several graph sizes $n \in [50, 400]$. Black and green dashed lines correspond to the Tracy-Widom distribution of type 1 and normal distributions, respectively. Each histogram was constructed from $10^6/n$ random graphs.

for small r , while $c_{\lambda_1, \lambda_2} \approx 0.53$ for $r \rightarrow \sqrt{2}$; see Fig. RGGs6.

- (vii) The distribution of the normalized distance between the first and second eigenvalues $P(s)$ and the distribution of the ratio between higher consecutive eigenvalues spacings $P(r)$ of randomly-weighted RGGs displays the PE-to-GOE transition as a function of $\langle k \rangle$. Moreover, for small [large] values of $\langle k \rangle$, the shapes of $P(s)$ and $P(r)$ are well described by $P_{\text{PE}}(s)$ and $P_{\text{PE}}(r)$ [$P_{\text{GOE}}(s)$ and $P_{\text{GOE}}(r)$], respectively; see Fig. RGGs7.
- (viii) The IPR distributions of all eigenvalues display a clear delocalization transition as $\langle k \rangle$ increases; see Fig. RGGs8. The IPR distributions of extreme eigenvalues (largest, second largest, and smallest) exhibit similar localization characteristics, in contrast with those for the bulk eigenvectors. Specifically, for small values of $\langle k \rangle$, the IPR distributions show a pronounced peak at $\text{IPR} = 3$, a signature of strongly localization and a characteristic of the PE. While for large values of $\langle k \rangle$ the IPR distributions follow a Gaussian-like bell shape centered at $\text{IPR} \propto N$, indicating delocalization which is the main characteristic of the GOE.

Acknowledgments

C.T.M.-M. Thanks for the support from CONAHCYT (CVU No. 784756). J.A.M.-B. Thanks for the support from VIEP-BUAP (Grant No. 100405811-VIEP2025), Mexico.

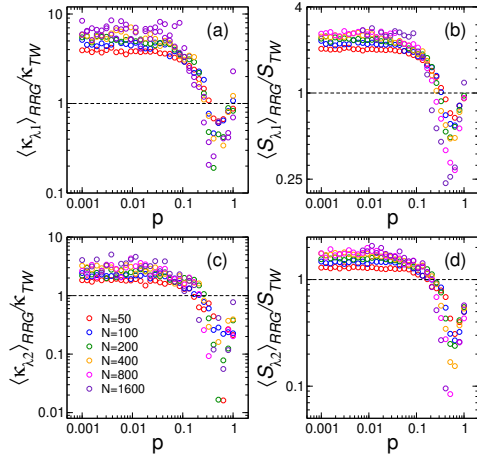


FIG. RGGs5: (a) [(c)] Excess kurtosis and (b) [(d)] skewness, normalized to the corresponding values of the Tracy-Widom distribution of type 1, for the largest eigenvalue λ_1 [for the second largest eigenvalue λ_2] as a function of the connection radius r of randomly-weighted random geometric graphs of sizes $n \in [50, 400]$. Each symbol was computed by averaging over $10^6/n$ random graphs.

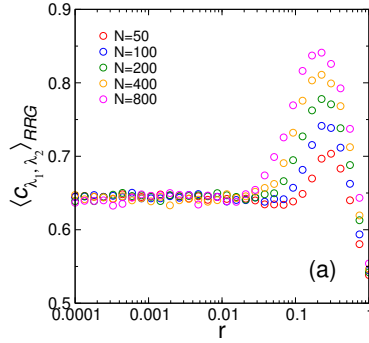


FIG. RGGs6: Correlation coefficient between the largest and the second largest eigenvalues as a function of the connection radius r of randomly-weighted random geometric graphs of sizes $n \in [50, 400]$. Each symbol was computed by averaging over $10^6/n$ random graphs.

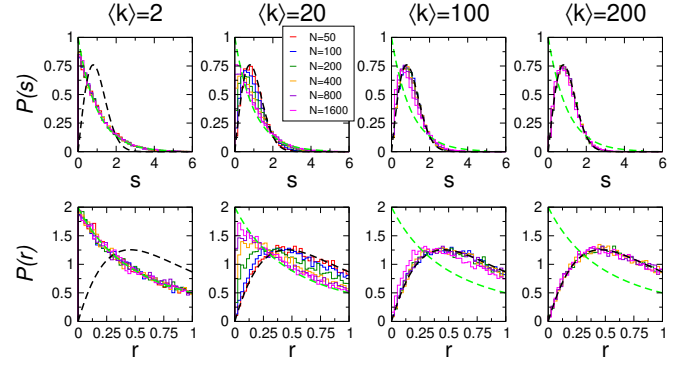


FIG. RGGs7: Top panels: Distribution of the normalized distance between the largest and second-largest eigenvalues $P(s)$ of randomly-weighted random geometric graphs for different values of $\langle k \rangle$, as indicated at the top of each panel. Bottom panels: Distribution of the ratio between higher consecutive eigenvalues spacings $P(r)$. Each panel displays histograms for different graph sizes, $n \in [50, 400]$. In the top panels, black and green dashed lines correspond to Eqs. (14) and (16), respectively. In the bottom panels, black and green dashed lines correspond to Eqs. (15) and (17), respectively. Each histogram was constructed from $10^6/n$ random graphs.

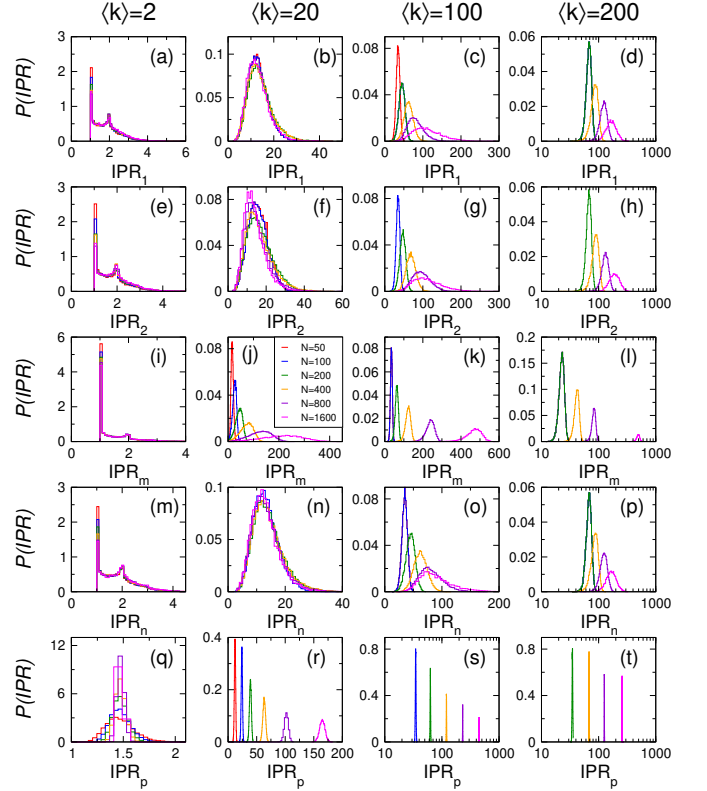


FIG. RGGs8: Distributions of inverse participation ratios $P(IPR)$ of eigenstates of randomly-weighted random geometric graphs of sizes $N \in [50, 800]$. Each column corresponds to a fixed value of $\langle k \rangle$. Rows are $P(IPR)$ of eigenstates corresponding to: (a-d) the largest eigenvalue, (e-h) the second largest eigenvalue, (i-l) the central eigenvalue ($m = N/2$), (m-p) the smallest eigenvalue, and (q-t) the average IPR over the full spectrum.

-
- [1] I. J. Farkas, I. Derényi, A. L. Barabási, and T. Vicsek, "Spectra of "real-world graphs": Beyond the semicircle law," *Phys. Rev. E* **64**(2), 026704 (2001).
- [2] S. Allesina and S. Tang, "Stability criteria for complex ecosystems," *Nature* **483**, 205–208 (2012).
- [3] M. Krivelevich and B. Sudakov, "The Largest Eigenvalue of Sparse Random Graphs," *Comb. Probab. Comput.* **12**, 61–72, (2003).
- [4] F. Chungh, L. Lu, V. Vu, "Spectra of random graphs with given expected degrees," *Proc. Natl. Acad. Sci. U.S.A.* **100**, 6313–6318, (2003).
- [5] E. Carro, L. Bennet, I. Pérez Castillo, "A smooth transition towards a Tracy-Widom distribution for the largest eigenvalue of interacting k-body fermionic Embedded Gaussian Ensembles", *J. Stat. Mech.* **2304**, 043201, (2023).
- [6] T. Belytschko, R. Mullen, "Stability of explicit-implicit mesh partitions in time integration," *Int. J. Numer. Methods Eng.*, **12**, 1575–1586 (1978).
- [7] M. Papadrakakis, "A method for the automatic evaluation of the dynamic relaxation parameters", *Comput. Methods Appl. Mech. Eng.* **25**, 35–48, (1981).
- [8] Q. Du, D. Wang, L. Zhu, "On mesh geometry and stiffness matrix conditioning for general finite element spaces," *SIAM J. Numer. Anal.* **47**, 1421–1444, (2009).
- [9] I. Fried, "Bounds on the extremal eigenvalues of the finite element stiffness and mass matrices and their spectral condition number," *J. Sound Vib.*, **22**, 407–418, (1972).
- [10] L. Laloux, P. Cizeau, J. P. Bouchaud, M. Potters, "Noise dressing of financial correlation matrices," *Phys. Rev. Lett.*, **83**, 1467, (1999).
- [11] V. Plerou, P. Gopikrishnan, B. Rosenow, L. A. N. Amaral, H. E. Stanley, "Universal and nonuniversal properties of cross-correlations in financial time series," *Phys. Rev. Lett.*, **83**, 1471, (1999).
- [12] M. Billio, M. Getmansky, A. W. Lo, L. Pelizzon, "Econometric measures of connectedness and systemic risk in the finance and insurance sectors," *J. financ. econ* **104**, 535–559, (2012).
- [13] P. W. Anderson, "Absence of diffusion in certain random lattices," *Phys. Rev.*, **109**, 1492, (1958).
- [14] O. Bohigas, M. J. Giannoni, C. Schmit, "Characterization of chaotic quantum spectra and universality of level fluctuation laws," *Phys. Rev. Lett.*, **52**, 1, C. (1984).
- [15] F. Evers, A. D. Mirlin, "Anderson transitions," *Rev. Mod. Phys.*, **80**, 1355–1417, (2008).
- [16] M. L. Mehta, *Random Matrices* (Elsevier, Amsterdam, 2004).
- [17] K.-I. Goh, B. Kahng, and D. Kim, "Spectra and eigenvectors of scale-free networks", *Phys. Rev. E* **64**, 051903, (2001).
- [18] F. Chung, *Spectral Graph Theory*, (American Mathematical Society, Providence, 1997).
- [19] A. Arenas, A. Díaz-Guilera, J. Kurths, Y. Moreno and C. Zhou, "Synchronization in complex networks," *Phys. Rep.* **469**, 93–153 (2008).
- [20] L. M. Pecora and T. L. Carroll "Master Stability Functions for Synchronized Coupled Systems," *Phys. Rev. Lett.* **80**, 2109 (1998).
- [21] M. Barahona and L. M. Pecora, "Synchronization in Small-World Systems," *Phys. Rev. Lett.* **89**, 054101, (2002).
- [22] C. Sarkar, and S. Jalan, "Spectral properties of complex networks," *Chaos*, **28**, 102101, (2018).
- [23] C. A. Tracy and H. Widom, "Distribution functions for largest eigenvalues and their applications," *arXiv preprint: arXiv:math-ph/0210034v2* (2002).
- [24] J. A. Mendez-Bermudez, A. Alcazar-Lopez, A. J. Martinez-Mendoza, F. A. Rodrigues and T. K. DM. Peron, "Universality in the spectral and eigenfunction properties of random networks", *Phys. Rev. E* **91**, 032122, (2015).
- [25] R. Aguilar-Sanchez, I. F. Herrera-Gonzalez, J. A. Mendez-Bermudez, and J. M. Sigarreta, "Computational properties of general indices on random networks", *Symmetry* **12**, 1341, (2020).
- [26] R. Aguilar-Sanchez, J. A. Mendez-Bermudez, F. A. Rodrigues, and J. M. Sigarreta, "Topological versus spectral properties of random geometric graphs", *Phys. Rev. E* **102**, 042306, (2020).
- [27] C. T. Martinez-Martinez, J. A. Mendez-Bermudez, J. M. Rodriguez, and J. M. Sigarreta-Almira, "Computational and analytical studies of the Randić index in Erdős-Rényi models", *Appl. Math. Comput.* **377**, 125137, (2020).
- [28] C. T. Martínez-Martínez, J. A. Méndez-Bermúdez, José M Rodríguez, José M Sigarreta, "Computational and analytical studies of the Harmonic index on Erdős-Rényi models", *Math. Comput. Chem.* **85**, 395, (2021).
- [29] T. Peron, de Resende Bruno Messias F., F. A. Rodrigues, L. D. F. Costa, and J. A. Méndez-Bermúdez, "Spacing ratio characterization of the spectra of directed random networks", *Phys. Rev. E* **102**, 062305, (2020).
- [30] K. Peralta-Martinez and J. A. Méndez-Bermúdez, "Directed random geometric graphs: structural and spectral properties", *J. Phys. Complex.* **4**, 015002, (2023).
- [31] C. T. Martinez-Martinez, J. A. Mendez-Bermudez, and J. M. Sigarreta-Almira, "Topological and spectral properties of random digraphs", *Phys. Rev. E* **109**, 064306, (2024).
- [32] J. A. Méndez-Bermúdez, A. Alcazar-López, A. J. Martínez-Mendoza, F. A. Rodrigues, and T. K. DM. Peron, "Universality in the spectral and eigenfunction properties of random networks," *Phys. Rev. E* **91**, 032122 (2015).
- [33] G. Torres-Vargas, J. A. Méndez-Bermúdez, J. C. Lopez-Vieyra, and R. Fossion, "Crossover in nonstandard random-matrix spectral fluctuations without unfolding," *Phys. Rev. E* **98**, 022110 (2018).
- [34] G. Torres-Vargas, R. Fossion, and J. A. Mendez-Bermudez, "Normal mode analysis of spectra of random networks," *Physica A*, in press (2020).
- [35] R. Aguilar-Sanchez, J. A. Mendez-Bermudez, J. M. Rodriguez, and J. M. Sigarreta-Almira, "Rodríguez-Velázquez indices on Erdős-Rényi graphs," submitted (2020).
- [36] E. P. Wigner, "On the distribution of the roots of certain symmetric matrices". *Ann. Math*, **67**, 325–327 (1958).
- [37] E. Estrada and M. Sheerin, "Random rectangular graphs," *Phys. Rev. E* **91**, 042805. (2015).